

Review

Hydrogen-Bonding Secondary Coordination Sphere Effect on CO₂ Reduction

Anamarija Briš *  and **Davor Margetić** 

Laboratory for Physical-Organic Chemistry, Division of Organic Chemistry and Biochemistry, Ruđer Bošković Institute, Bijenička c. 54, 10000 Zagreb, Croatia

* Correspondence: abris@irb.hr

Abstract: Great efforts of the scientific community are focused on the development of catalysts for the reduction of carbon dioxide (CO₂) to useful molecules such as carbon monoxide, formic acid, methanol, ethanol, methane, ethylene, or acetate. Various metal porphyrin complexes were synthesized and studied to develop highly active and selective catalysts. While the substituents on the porphyrin core (the primary coordination sphere) determine the reactivity of the metal, the introduction of the secondary coordination is important for the binding and activation of CO₂. In this review, selected examples of iron porphyrin catalysts with a secondary coordination sphere capable of stabilizing intermediates of the CO₂ reduction process by hydrogen bonding are presented.

Keywords: carbon dioxide; reduction; electrocatalysts; iron porphyrin; secondary coordination sphere; hydrogen bonding

1. Introduction

The concentration of carbon dioxide (CO₂) in the atmosphere is steadily increasing (Figure 1) [1] and its accumulation is causing many harmful climate changes such as global warming, mass loss of the land ice sheets in both Antarctica and Greenland, sea level rise, expansion of deserts, and more, all of which directly affect the sustainability of life on Earth. Natural consumption of CO₂ is not enough to reduce CO₂ levels in the atmosphere. Therefore, many efforts are focused on converting CO₂ into useful molecules through chemical methods [2].



Citation: Briš, A.; Margetić, D. Hydrogen-Bonding Secondary Coordination Sphere Effect on CO₂ Reduction. *Organics* **2023**, *4*, 277–288. <https://doi.org/10.3390/org4020022>

Academic Editor: Michał Szostak

Received: 24 March 2023

Revised: 23 April 2023

Accepted: 31 May 2023

Published: 5 June 2023



Copyright: © 2023 by the authors. Licensee MDPI, Basel, Switzerland. This article is an open access article distributed under the terms and conditions of the Creative Commons Attribution (CC BY) license (<https://creativecommons.org/licenses/by/4.0/>).

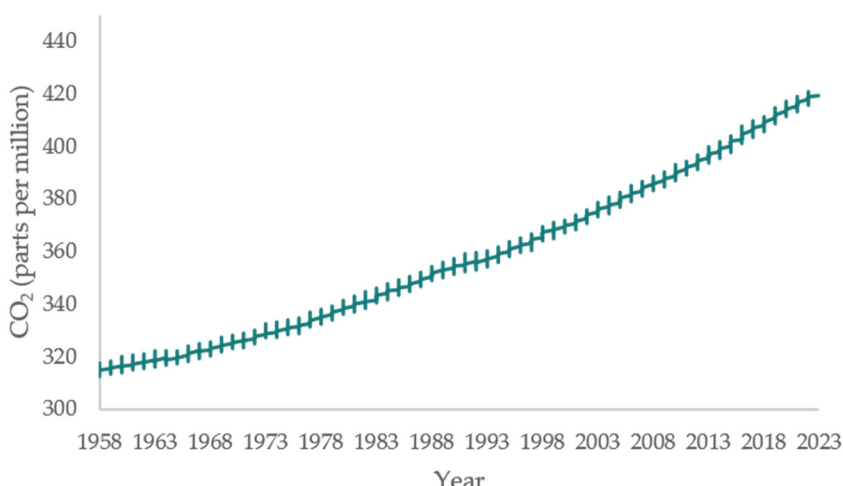
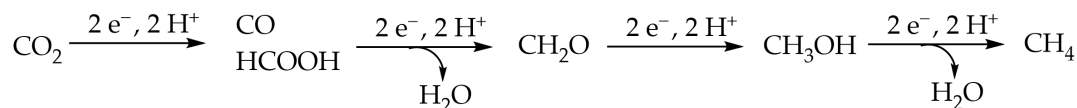


Figure 1. The increase of CO₂ level from 1958 to the present [1].

The problem in CO₂ conversion is the very high thermodynamic stability of CO₂ and electrocatalytic reduction showed promising results [3,4]. The conversion of CO₂ into

useful molecules consists of a combination of reduction and protonation, which leads to several different mono-carbon (C_1) molecules such as carbon monoxide, formic acid, formaldehyde, methanol, and methane (Scheme 1) as well as multi-carbon (C_{2+}) products such as ethylene, ethanol, etc. [2,5].



Scheme 1. Possible C₁ products of CO₂ reduction.

The requirement for efficient catalysts is high activity and selectivity in CO₂ reduction. In nature, there are various examples of small molecules activation and conversion by tetrapyrrole-based macrocycles, e.g., heme, the iron complex of porphyrin, which is very important for the binding, transport, storage, and activation of oxygen in various proteins and enzymes [6]; siroheme, the iron complex of isobacteriochlorin, which catalyzes the reduction of nitrite and sulfite [7]. Mimicking nature, scientists have developed numerous metal porphyrinoid complexes capable of electrocatalytically reducing CO₂ [8]. The possibility of substitution of both *meso*- and β -positions of the porphyrin (Figure 2a), and complexation with different metals allows a wide range of catalyst modifications and the study of their effects on the efficiency and selectivity of CO₂ reduction.

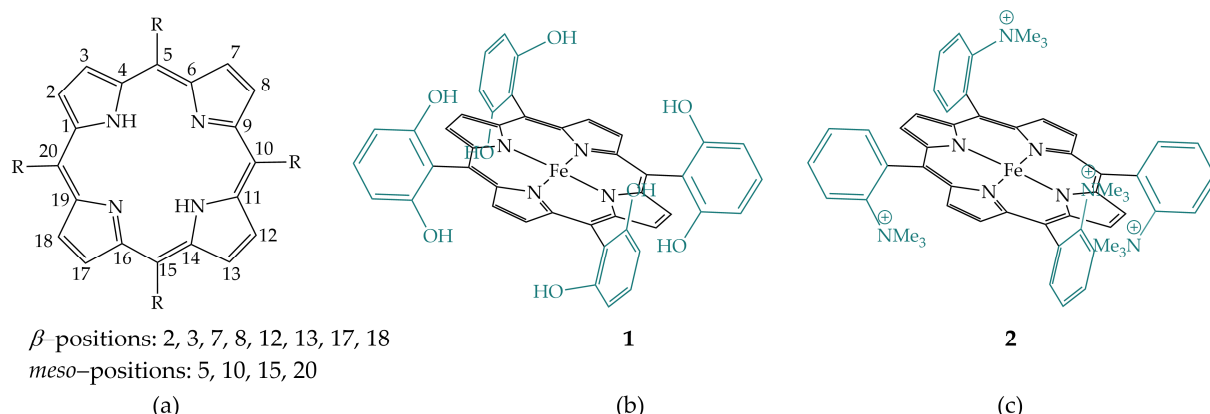


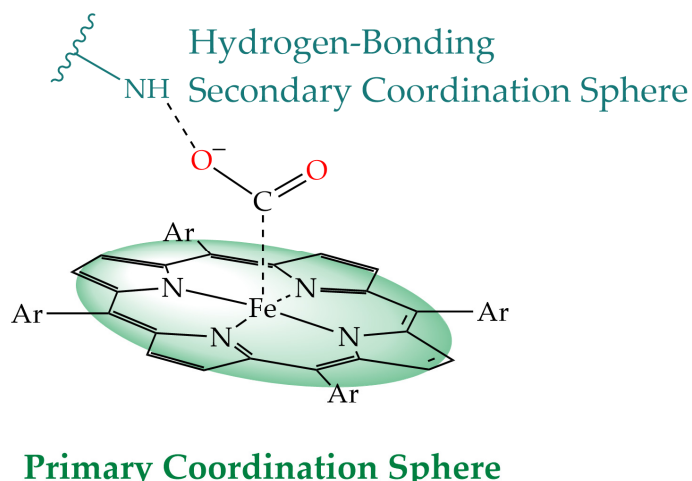
Figure 2. (a) Porphyrin structure with denoted *meso*- and β -positions; (b) Iron 5,10,15,20-tetrakis(2',6'-dihydroxyphenyl)-porphyrin; (c) Iron tetraphenylporphyrin with four trimethylanilinium groups.

Iron porphyrins show promising results for the reduction of CO₂ to CO [9]. Many mechanistic studies have been carried out [4,10]. Iron porphyrins bind CO₂ in its Fe(0) state, whereupon subsequent proton and electron transfer and release of CO occur. Through-structure substituent effect (the primary coordination sphere) stabilizes the reduced metal and determines the reactivity of the metal. The introduction of the secondary coordination sphere improves the stability of the CO₂ reduction intermediates, which directly affects the selectivity and rate of reduction [11–13].

Savéant et al. made a systematic study of the substitution effects on electrochemical CO₂ reduction catalyzed by iron porphyrins. The introduction of phenolic groups, a local proton source, in all *ortho* and *ortho'* positions of the phenyl groups of porphyrin, leads to enhanced activity of iron porphyrin (Figure 2b) [14]. Their investigation of the effects of the primary coordination sphere by the introduction of electron-withdrawing and electron-donating substituents with successive phenyl perfluorination and the *o,o'*-methoxy substitution of iron tetraphenylporphyrin [15] as well as the effects of the secondary coordination sphere by the introduction of positive charges, the four trimethylanilinium groups, and negative charges, the four sulfonate groups, on the phenyl rings of iron tetraphenylporphyrin, led to the excellent performing catalyst 2, showing very high selec-

tivity for the reduction of CO_2 to CO with a maximum turnover frequency (TOF) of 10^6 s^{-1} (Figure 2c) [16].

Various strategies have been used for the secondary coordination sphere such as the introduction of local proton sources, hydrogen bond donors, cationic moieties, and bimetallic approach [13]. In this review, examples of iron porphyrin electrocatalysts with ligands that stabilize intermediates by hydrogen bonding are selected (Figure 3).



Primary Coordination Sphere

Figure 3. Representation of primary and hydrogen-bonding secondary coordination sphere.

2. Hydrogen-Bonding Secondary Coordination Sphere Effect

As a general mechanism for CO_2 reduction to CO by iron (III) tetraphenylporphyrin (**FeTPP**), **FeTPP** undergoes three reversible reductions that correspond to reductions from Fe(III) to Fe(II) to Fe(I) and to Fe(0), the active form that reacts with CO_2 [17].

Iron porphyrins with hydrogen bonding groups in the secondary coordination sphere form hydrogen bonding interactions with at least two intermediates of reduction, an Fe(II) $-\text{CO}_2^{2-}$ and an Fe(II) $-\text{COOH}$ species, which affect their stability and influence both the selectivity and the rate of CO_2 reduction [18]. The Fe(II) $-\text{CO}_2^{2-}$ species is very basic and can be easily protonated by a weak acid to generate Fe(II) $-\text{COOH}$ species. In the presence of a strong acid, protonation of Fe(II) $-\text{COOH}$ species leads to $-\text{OH}$ protonation, elimination of water, and formation of Fe(II) $-\text{CO}$. In the presence of a weak acid, C-protonation of the Fe(II) $-\text{COOH}$ species occurs and formate is released. The rate-determining step is a bond cleavage of the Fe(II) $-\text{COOH}$ species. Hydrogen-bonding residues are also able to form hydrogen bonds with external proton sources, which bring them close to the CO_2 reduction intermediates and synergistically activate them. Iron porphyrins are functionalized with various hydrogen bonding groups such as amides, phenols, guanidines, triazoles, ureas, pyridines, amines or imidazoles.

2.1. Amides in the Secondary Coordination Sphere

Nichols et al. investigated the secondary sphere effects of positional isomers of iron porphyrins having pendant amide in the *ortho* or *para* position of the phenyl ring, proximal or distal to the porphyrin macrocycle (Figure 4) in dimethylformamide (DMF) in the presence of phenol (PhOH) as an acid source [19]. All four porphyrin derivatives reduce CO_2 to CO. Compared to **FeTPP**, *ortho* derivatives **3** and **4** show an increase in CO_2 reduction rate due to secondary sphere interactions, while secondary sphere effects are absent in *para* derivatives **5** and **6**. Moreover, the effects are more pronounced in the porphyrin **4** when the amide group is distal to the porphyrin macrocycle.

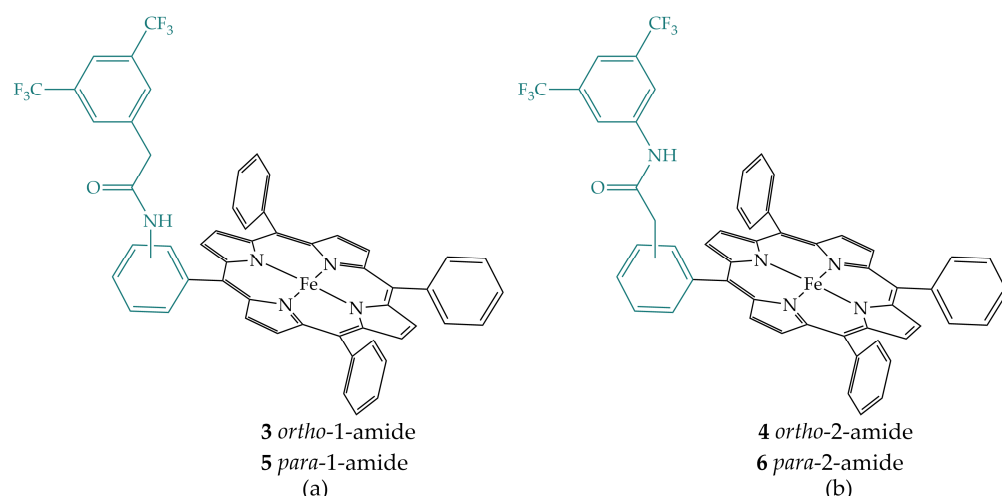


Figure 4. (a) *ortho*- and *para*-1-amide iron porphyrins **3** and **5**; (b) *ortho*- and *para*-2-amide iron porphyrins **4** and **6**.

2.2. Phenols and Guanidines in the Secondary Coordination Sphere

Margarit et al. synthesized iron porphyrins having phenolic (7) and guanidyl (8) groups in the secondary coordination sphere (Figure 5), hanging above the iron porphyrin macrocycle, which reduce CO_2 to CO with Faradaic efficiencies of more than 93% [20]. Computational studies of CO_2 binding to the reduced iron porphyrin Fe(0), showed thermodynamically more stable binding within hangman cleft due to hydrogen bonding for both porphyrins compared to the other side of the porphyrin macrocycle. A stronger association is observed for porphyrin with the phenolic group, which is also consistent with a higher rate constant compared to that with the guanidyl group. Computational studies also showed that both complexes have hydrogen bonding of the hanging group to the porphyrin prior to CO_2 binding [20]. The phenolic group binds to the iron and nitrogen of the pyrrole, while the guanidyl group binds to the α and β carbon atoms of the pyrrole and is thus further away from the metal center, implying that upon CO_2 binding, the backbone of the hanging group must rotate to accommodate CO_2 .

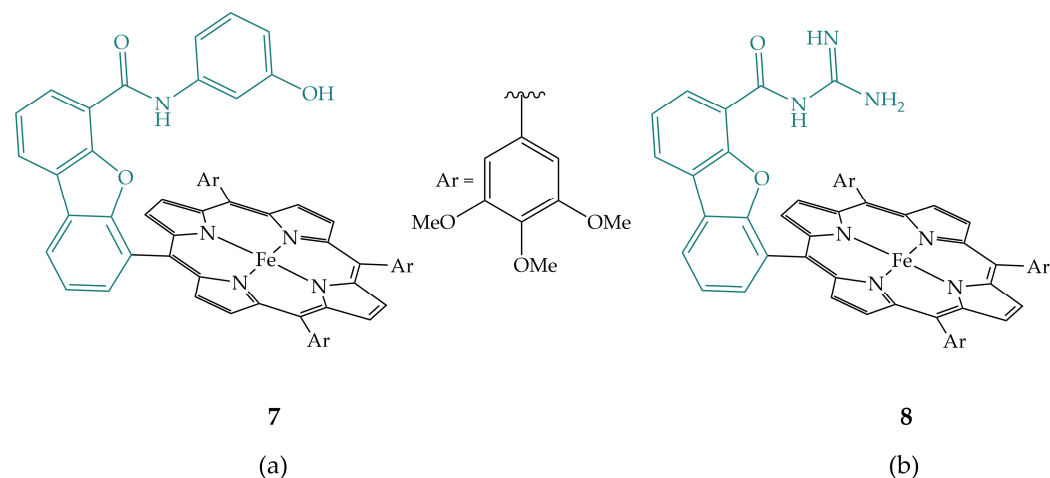


Figure 5. Iron hangman porphyrins with (a) phenolic (7) and (b) guanidyl group (8).

Guo et al. synthesized porphyrin **9** (Figure 6), which also has a phenolic group hanging directly over the iron porphyrin macrocycle and investigated its electrocatalytic activity in CO_2 reduction in comparison to its analogue, non-functionalized porphyrin **10** (Figure 6) [21]. Furthermore, the activity of porphyrins with two different counter ions, chloride ($-\text{Cl}$) and triflate ($-\text{OTf}$) was investigated. They were unable to obtain crystals

suitable for X-ray structural analysis, but according to published data on various iron porphyrins, they assume that Fe(III) is incorporated in the center of the porphyrin macrocycle with a counter ion as an axial ligand as shown for the other porphyrin derivatives. Their studies showed that the chloride salt of porphyrin **9-Cl** is much less active compared to porphyrin **10-Cl** due to the hydrogen bonding of the axial chloride with the phenolic group. Switching to the triflate salt, **9-OTf** is more active than both **9-Cl** and **10-Cl**. **10-OTf** has the same activity as **10-Cl**. Thus, iron porphyrin **9** shows an activity dependence on the counter ions and in addition to the positive secondary coordination sphere effect of the phenolic group in the CO₂ reduction reaction, as shown above for the porphyrin **7**, the phenolic group in porphyrin **9** also has an inhibitory effect, depending on the counter ion used.

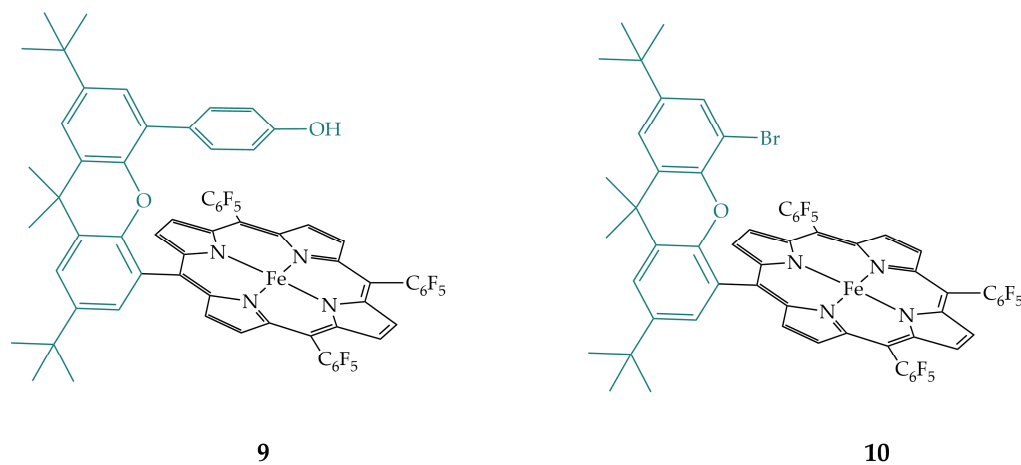


Figure 6. Iron porphyrin with phenolic group **9** and its non-functionalized analogue, iron porphyrin **10**.

In addition, Guo et al. synthesized porphyrin **11** (Figure 7) with the pendant guanidyl group and compared its electrocatalytic activity and selectivity for CO₂ reduction with its non-functionalized analogue tetrakis(3,4,5-trimethoxyphenyl)porphyrin **12** (Figure 7) [22]. In acetonitrile with added water, both show the same selectivity for CO₂ reduction to CO, but porphyrin **11** is much more active than its analogue **12**, with a TOF value that is an order of magnitude higher. In aqueous solutions, porphyrin **11** is much more active and selective than porphyrin **12** with a Faradaic efficiency of 96%, while porphyrin **12** has a Faradaic efficiency of 65% for CO₂ reduction to CO. The guanidyl group of porphyrin **11** is protonated in an aqueous solution; therefore, it can stabilize intermediates of CO₂ reduction and act as a proton relay.

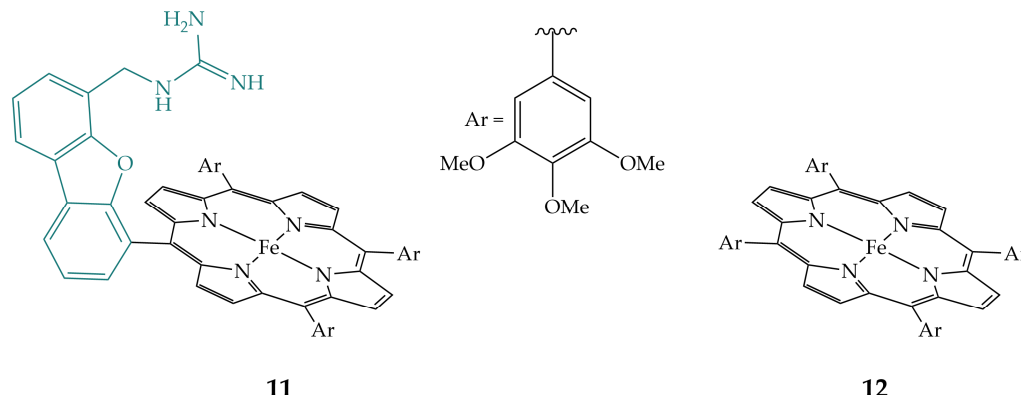


Figure 7. Iron porphyrin with guanidyl group **11** and its non-functionalized analogue, iron porphyrin **12**.

2.3. Triazoles in the Secondary Coordination Sphere

Sen et al. studied CO₂ reduction with three iron porphyrins that differ in hydrogen bonding residues in the secondary coordination sphere with the same external acid, with porphyrin **13** having an amide, a hydrogen bond donor, while porphyrins **14** and **15** have hydrogen bond acceptors, 4-*tert*-butyltriazole and 4-methylcarboxylatetraazole groups, respectively, that are able to entrap water molecules (Figure 8) [23]. Porphyrins are derivatized in the *ortho* position of the phenyl ring. In addition, the pivaloyl groups of porphyrin **13** provide a hydrophobic environment, while the groups of porphyrins **14** and **15** provide a hydrophilic environment. All three porphyrins showed a reduction of CO₂ to CO but with different values: 1 s⁻¹, 4.2 s⁻¹, and 2 × 10³ s⁻¹ for iron porphyrin **15**, **14**, and **13**, respectively (with respect to the rate of porphyrin **15** set to 1). Their study showed that it is possible to affect CO₂ reduction rates only by regulating electrostatics and hydrogen bonding interactions, while hydrophobicity does not have much effect on it.

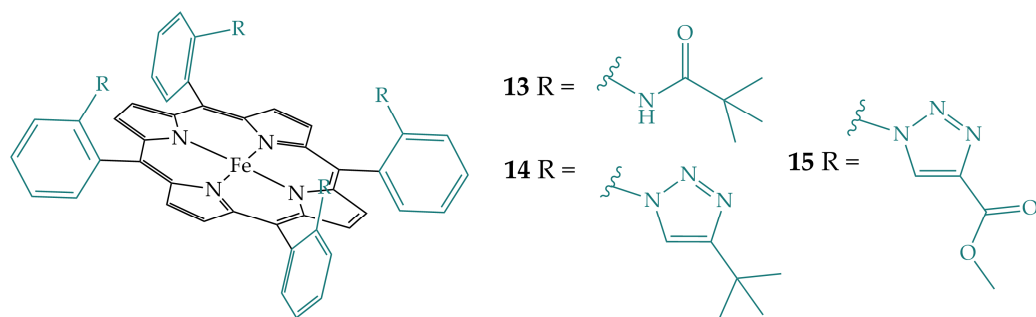


Figure 8. Iron porphyrins with amide (**13**), 4-*tert*-butyltriazole (**14**), and 4-methylcarboxylatetraazole (**15**) groups.

2.4. Ureas in the Secondary Coordination Sphere

Gotico et al. designed iron porphyrin derivative **16**, which has amide groups in the secondary coordination sphere, and compared its electrocatalytic activity with iron porphyrin derivative **17**, which has urea groups, opening the possibility of multipoint hydrogen bonding interactions (Figure 9a) [24]. Both porphyrins are derivatized in the *ortho* position of all phenyl rings with an $\alpha\beta\alpha\beta$ configuration. They showed an improvement in electrocatalytic activity for both iron porphyrins **16** and **17** compared to FeTPP, while a stronger improvement was observed for porphyrin **17** with urea functionalities. A controlled experiment with FeTPP and the addition of external urea showed no enhancement, highlighting the importance of the pre-organized structure of the iron porphyrin derivative. DFT calculations confirmed two weak hydrogen bonds of the amide groups with CO₂ in porphyrin **16** and four strong interactions with urea groups in porphyrin **17**. The electrocatalytic activity was studied in DMF using water as a proton source, which turned out to be a better proton source than the more acidic trifluoroethanol (TFE) or phenol. Water acts in synergy with urea groups. Computational studies confirmed the possibility of complexed water molecules with hydrogen bonds between the CO₂ and urea groups. Gotico et al. also studied the electrocatalytic activity of porphyrins with two urea groups in $\alpha\alpha$ (**18**) and $\alpha\beta$ (**19**) configurations (Figure 9b), where one side of the metal remains free after CO₂ binding [25]. $\alpha\alpha$ porphyrin **18** showed higher binding affinity towards CO₂ but $\alpha\beta$ porphyrin **19** showed higher electrocatalytic activity. In the latter complex, the approach of water is easier due to the $\alpha\beta$ configuration, so the proton transfer process is faster.

In addition, Derrick et al. functionalized iron porphyrin with one urea group in the *ortho* position (porphyrin **20**), and *para* position (porphyrin **21**) of the porphyrin phenyl ring and investigated electrochemical CO₂ reduction with bicarbonate as an additive (Figure 9c) [26]. Bicarbonate serves as a proton donor and its interaction with the urea group through hydrogen bonding increases its acidity and brings it close to the CO₂-bonded intermediate, resulting in rapid proton transfer and an increase in the catalytic

rate of electrochemical CO_2 reduction. The increase is more pronounced for the *ortho*-functionalized porphyrin **20**.

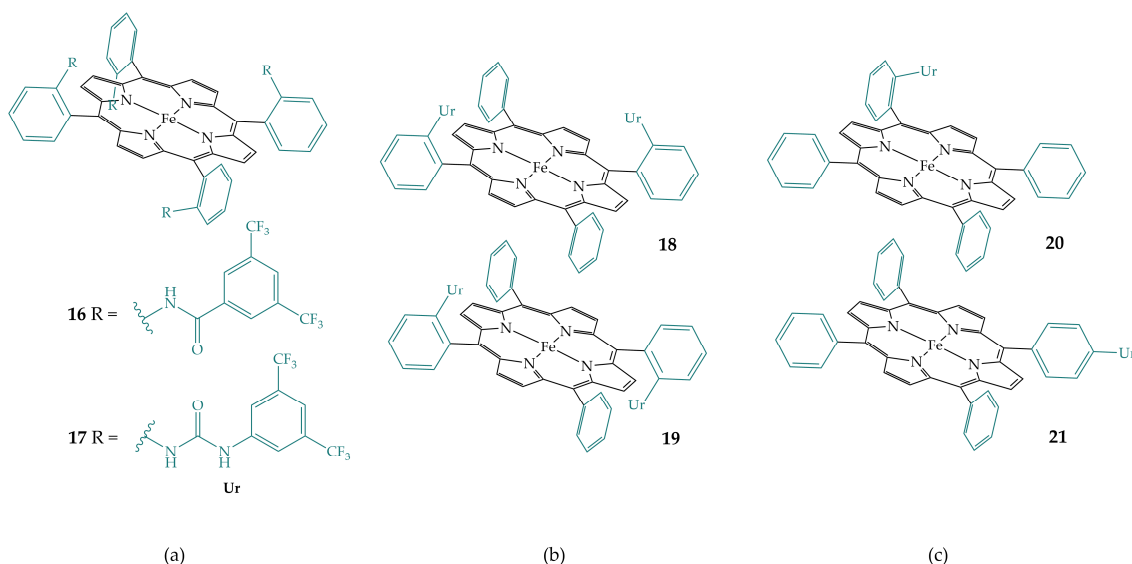


Figure 9. (a) Iron porphyrins with four amide (**16**) and urea (**17**) groups with an $\alpha\beta\alpha\beta$ configuration; (b) Iron porphyrins with two urea groups with $\alpha\alpha$ (**18**) and $\alpha\beta$ (**19**) configurations; (c) Iron porphyrins with one urea group in *ortho* position (**20**), and *para* position (**21**).

2.5. Amines in the Secondary Coordination Sphere

Liu et al. studied electrochemical CO_2 reduction with simple iron porphyrins bearing an amino group in the *ortho* position, iron 5-(*o*-aminophenyl)-10,15,20-triphenylporphyrin (**22**) and the *para* position, iron 5-(*p*-aminophenyl)-10,15,20-triphenylporphyrin (**23**) (Figure 10a) [27]. In this study, as with the *ortho* iron porphyrin derivatives **2** and **3** mentioned above, the *ortho*-substituted porphyrin **22** showed better TOF, lower overpotential, and higher selectivity, compared to the *para*-substituted iron porphyrin **23**. DFT calculations showed stabilization of $\text{Fe}(\text{II})-\text{CO}_2^{2-}$ species forming hydrogen bond interactions with the amino group.

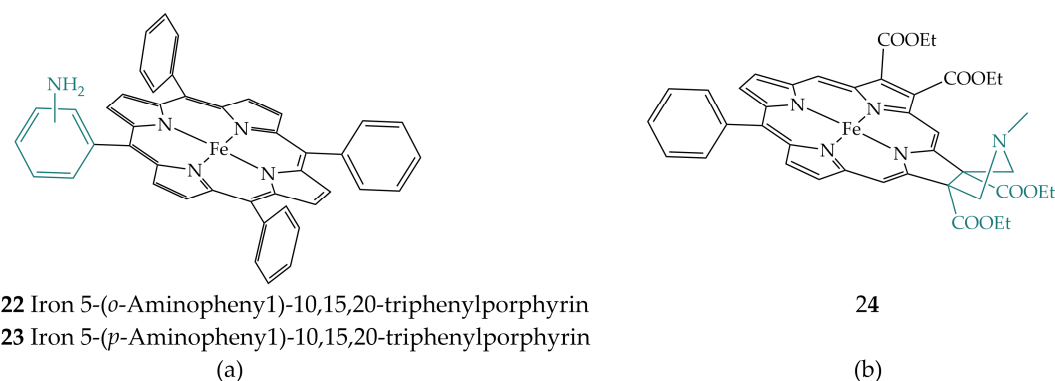


Figure 10. (a) Iron 5-(*o*-Aminophenyl)-10,15,20-triphenylporphyrin (**22**) and iron 5-(*p*-Aminophenyl)-10,15,20-triphenylporphyrin (**23**); (b) Iron porphyrin with a rigid pendant amine group **24**.

Amanullah et al. tuned the CO_2 reduction to produce HCOOH . The reduction was catalyzed with iron porphyrinoid **24**, which has a rigid pendant amine (Figure 10b), in DMF with water as the proton source [28]. In contrast to the above examples, iron porphyrinoid **24** can activate CO_2 in its $\text{Fe}(\text{I})$ state, thereby lowering the overpotential of the process. The pendant amine is located near the active site and after its protonation, CO_2 binding to $\text{Fe}(\text{I})$ is possible as well as stabilization of $\text{Fe}(\text{III})-\text{COOH}$ and $\text{Fe}(\text{II})-\text{COOH}$ species.

Guo et al. synthesized four porphyrins differing in the number of *N,N,N*-trimethylbenzylamine groups, porphyrin **25** with two groups in *cis* position, porphyrin **26** with two groups in *trans* position, porphyrin **27** with one group, and the non-functionalized analogue, porphyrin **28** (Figure 11) [29]. Porphyrin **25** showed the best electrocatalytic activity for CO₂ reduction to CO in acetonitrile using phenol as a proton source, followed by porphyrin **26**, porphyrin **27**, and porphyrin **28**. Therefore, functionalization of iron porphyrin with *N,N,N*-trimethylbenzylamine groups increased the activity compared to non-functionalized porphyrin. The *cis*-isomer has the best stabilization of the CO₂-bonded intermediate by both electrostatic and hydrogen bonding and promotes better rate-determining C–O bond cleavage due to cooperative interactions with both an Fe(II)–COOH intermediate and phenol.

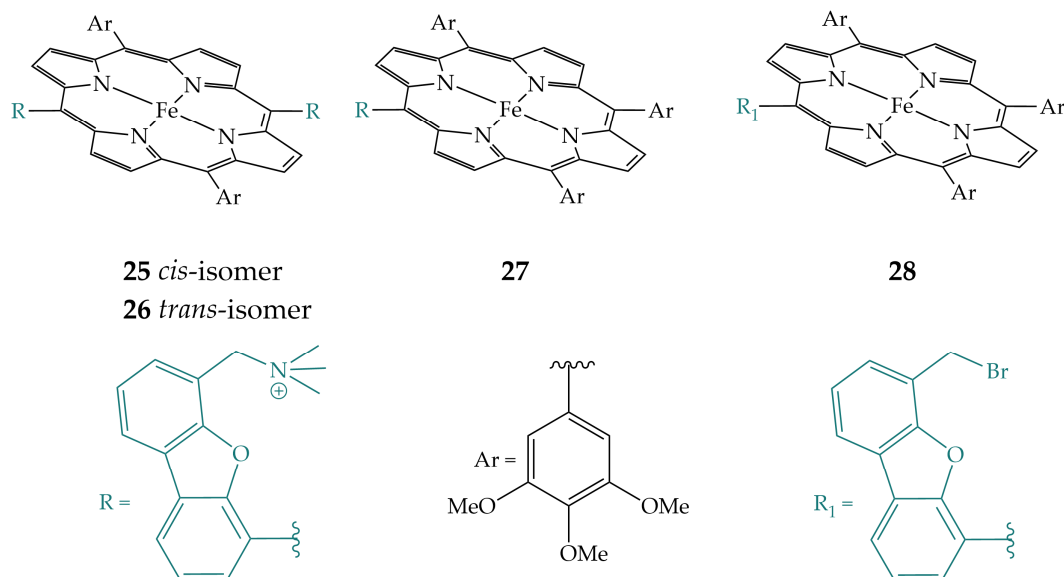


Figure 11. Iron porphyrins with *N,N,N*-trimethylbenzylamine groups **25**, **26**, **27**, and non-functionalized analogue, iron porphyrin **28**.

2.6. Pyridines in the Secondary Coordination Sphere

Ramuglia et al. provided iron porphyrin (**29**) with pendant pyridine substituents (Figure 12) and compared its electrocatalytic activity with a non-functionalized tetramesitylporphyrin (**30**) in acetonitrile with the addition of the weak acids [30]. Porphyrin **29** showed an increased reduction rate compared to non-functionalized porphyrin **30**, which can be attributed to the hydrogen bonding interactions of the pyridine substituents assisting in the proton transfer to the one-electron reduced CO₂ adduct or stabilization of the Fe(II)–COOH species.

2.7. Imidazoles in the Secondary Coordination Sphere

Narouz et al. synthesized a series of iron porphyrins with pendant imidazolium ligands in the *ortho* position (porphyrins **31** and **33**) and *para* position (porphyrin **32**) of the porphyrin phenyl rings (Figure 13) [31]. The imidazolium pendant ligands in porphyrins **31** and **32** could enhance the stabilization of the intermediates of CO₂ reduction by both electrostatic and hydrogen bonding interactions, while porphyrin **33** has no hydrogen bonding interactions. In this way, both position tuning and the effects of electrostatic and hydrogen bonding interactions on the activity of the reduction reaction can be compared. The best performance was obtained with porphyrin **31** in both acetonitrile and aqueous media, followed by porphyrin **33** and porphyrin **32**. Porphyrin **31** showed a 5-fold increase in CO₂ binding affinity over porphyrin **33**, a 20-fold increase over porphyrin **32**, and a 25-fold increase in CO₂ binding affinity compared to FeTPP, demonstrating the importance of the introduction of the secondary coordination sphere as well as proper positioning in

the secondary coordination sphere. The TOF values are also much higher for porphyrin 31 compared to porphyrin 32 and **FeTPP**, an increase of several thousand, but only slightly higher than for porphyrin 33, indicating the dominance of the electrostatic effect in the catalytic enhancement. In addition, porphyrins 31 and 33 are more selective for CO₂ reduction to CO compared to porphyrin 32.

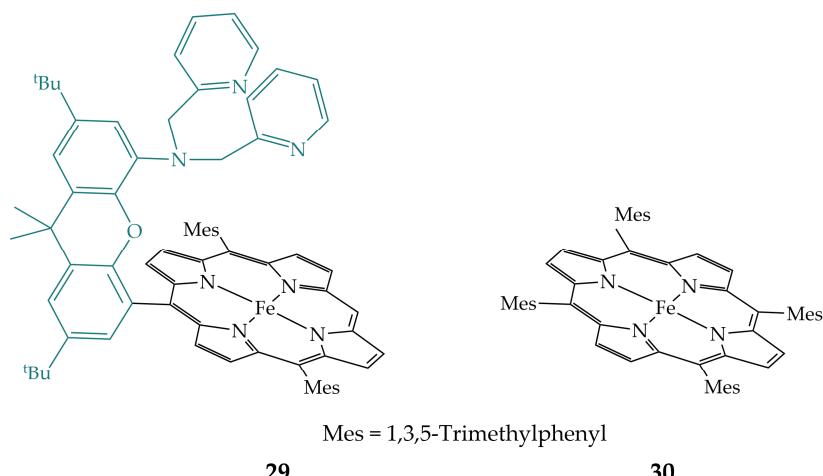


Figure 12. Iron porphyrin with pendant pyridine substituents **29** and non-functionalized analogue **30**.

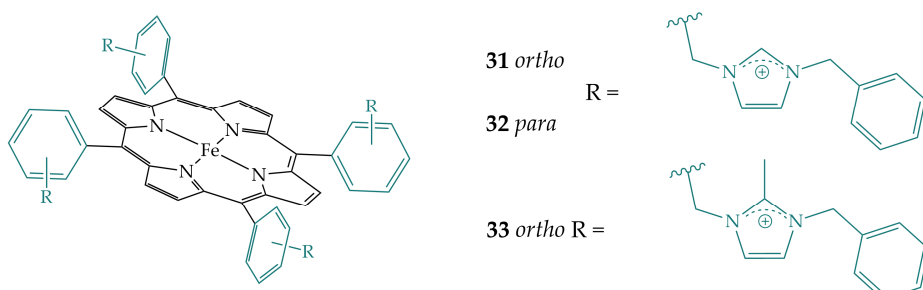


Figure 13. Iron porphyrins with pendant imidazolium substituents.

2.8. Summary of Data for Iron Porphyrins

The iron porphyrins discussed above and their electrochemical properties are summarized in Table 1. The detailed description of the foot-of-the-wave (FOW) analysis and the estimation of the TOF values are described elsewhere [12,32]. Plotting the log TOF against the overpotential (η) estimated based on the catalytic parameters by the FOW analysis yields a catalytic Tafel plot (Figure 14). The compilation of catalytic Tafel plots for different porphyrins in one diagram allows a quick comparison of the catalytic activity with effective electrocatalysts located in the upper left part of the plot having large TOF_{\max} at a low overpotential of the system.

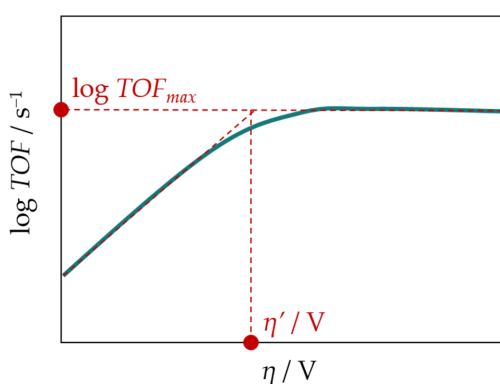


Figure 14. Representation of a catalytic Tafel plot.

Table 1. Iron porphyrins, overpotential (η')¹, the standard potential of the reversible reduction peak of the active form of the catalyst (E_{cat}^0)¹, log TOF_{max} values and Faradaic efficiency (FE) for CO production.

Porphyrin	Conditions	η'/V	E_{cat}^0/V	log TOF _{max} /s ⁻¹	FE/%	Ref.
FeTPP	DMF + 3 M PhOH	0.74		4.5	87	[16]
1	DMF + 2 M H ₂ O	0.64		6.0	94	[12,14]
2	DMF + 3 M PhOH	0.22		6.0	~100	[16]
3	DMF + 0.1 M PhOH		−2.12 ²	4.4	83	[19]
4	DMF + 0.1 M PhOH		−2.18 ²	6.7	92	[19]
5	DMF + 0.1 M PhOH		−2.15 ²	2.2	74	[19]
6	DMF + 0.1 M PhOH		−2.16 ²	3.8	79	[19]
7	DMF + 0.04 M PhOH	0.76		2.7	94	[20]
8	DMF + 0.04 M PhOH	0.77		2.5	93	[20,33]
11	ACN + 0.25 M H ₂ O			5.6	98	[22]
12	ACN + 0.25 M H ₂ O			4.2	96	[22]
13	ACN + 3 M PhOH		−1.27 ³	5.7	87	[23]
14	ACN + 3 M PhOH		−1.19 ³	3.0		[23]
15	ACN + 3 M PhOH		−1.15 ³	2.4		[23]
16	DMF + 5 M H ₂ O	0.63		3.85		[24]
17	DMF + 5 M H ₂ O	0.43		3.83	91	[24]
18	DMF + 2.22 M H ₂ O	0.56		4.08	91	[25]
19	DMF + 2.22 M H ₂ O	0.61		4.71	95	[25]
20	DMF + 0.1 M TEAHCO ₃		−2.06 ²		93	[26]
21	DMF + 0.1 M TEAHCO ₃		−2.18 ²		54	[26]
22	DMF + 1 M PhOH	0.76		4.0	88	[27]
23	DMF + 1 M PhOH	0.82		3.4	87	[27]
24	DMF + 1 M H ₂ O		−1.55 ⁴	2.2	97 ⁴	[28]
25	ACN + 0.25 M PhOH		−1.82 ⁵	5.6	95	[29]
26	ACN + 0.25 M PhOH		−1.88 ⁵	5.4	93	[29]
27	ACN + 0.25 M PhOH		−1.98 ⁵	5.0	93	[29]
28	ACN + 0.25 M PhOH		−2.05 ⁵	4.3	91	[29]
29	ACN + 0.128 M PhOH	0.95		8.3		[30]
30	ACN + 0.128 M PhOH	0.86		6.9		[30]
31	ACN + 3 M TFE		−1.78 ²	9.1	100	[31]
32	ACN + 3 M TFE		−1.79 ²	4.9	28	[31]
33	ACN + 3 M TFE		−1.79 ²	7.5	100	[31]

¹ $\eta' = E_{CO_2/CO}^0 - E_{cat}^0$; E_{cat}^0 the standard reduction potential for the formal Fe^{I/0} couple. ² E_{cat}^0 (V vs. Fc/Fc⁺).

³ E_{cat}^0 (V vs. NHE). ⁴ E_{cat}^0 for the formal Fe^{II/I} couple; FE for HCOOH production. ⁵ Onset potential, E (V vs. Fc/Fc⁺).

3. Conclusions

CO₂ can be catalytically reduced to various products. The selectivity of the reaction is very important for the further use of these products. In this review, iron porphyrin electrocatalysts with hydrogen bonding residues in the secondary coordination sphere are presented. It is shown how a simple modification of iron porphyrin can improve the rate and selectivity of CO₂ reduction compared to FeTPP by stabilizing reduction intermediates through hydrogen bonding as well as hydrogen bonding interactions with external proton sources. Nevertheless, the precise positioning, as well as the strength of hydrogen bonding interactions are very important. Further improvements are needed to increase electrocatalytic activity, reduce side products like molecular hydrogen, and tune the reduction to produce multi-carbon (C₂₊) products.

Author Contributions: Idea, conceptualization, literature search, writing—original draft preparation, visualization, A.B.; writing—review and editing, D.M. All authors have read and agreed to the published version of the manuscript.

Funding: This research received no external funding.

Data Availability Statement: Not applicable.

Conflicts of Interest: The authors declare no conflict of interest.

References

- Carbon Dioxide. National Oceanic and Atmospheric Administration. Available online: <https://climate.nasa.gov/> (accessed on 6 March 2023).
- Kinzel, N.W.; Werlé, C.; Leitner, W. Transition Metal Complexes as Catalysts for the Electroconversion of CO₂: An Organometallic Perspective. *Angew. Chem. Int. Ed.* **2021**, *60*, 11628–11686. [[CrossRef](#)]
- Pappijn, C.A.R.; Ruitenbeek, M.; Reyniers, M.-F.; Van Geem, K.M. Challenges and Opportunities of Carbon Capture and Utilization: Electrochemical Conversion of CO₂ to Ethylene. *Front. Energy Res.* **2020**, *8*, 557466.
- Francke, R.; Schille, B.; Roemelt, M. Homogeneously Catalyzed Electroreduction of Carbon Dioxide—Methods, Mechanisms, and Catalysts. *Chem. Rev.* **2018**, *118*, 4631–4701. [[CrossRef](#)] [[PubMed](#)]
- Li, D.; Zhang, H.; Xiang, H.; Rasul, S.; Fontmorin, J.-M.; Izadi, P.; Roldan, A.; Taylor, R.; Feng, Y.; Banerji, L.; et al. How to Go Beyond C₁ Products with Electrochemical Reduction of CO₂. *Sustain. Energy Fuels* **2021**, *5*, 5893–5914. [[CrossRef](#)]
- Zhang, W.; Lai, W.; Cao, R. Energy-Related Small Molecule Activation Reactions: Oxygen Reduction and Hydrogen and Oxygen Evolution Reactions Catalyzed by Porphyrin- and Corrole-Based Systems. *Chem. Rev.* **2017**, *117*, 3717–3797. [[CrossRef](#)]
- Amanullah, S.; Saha, P.; Dey, A. Recent Developments in the Synthesis of Bio-Inspired Iron Porphyrins for Small Molecule Activation. *Chem. Commun.* **2022**, *58*, 5808–5828. [[CrossRef](#)] [[PubMed](#)]
- Dedić, D.; Dorniak, A.; Rinner, U.; Schöfberger, W. Recent Progress in (Photo-)Electrochemical Conversion of CO₂ With Metal Porphyrinoid-Systems. *Front. Chem.* **2021**, *9*, 685619. [[CrossRef](#)]
- Bhugun, I.; Lexa, D.; Savéant, J.-M. Catalysis of the Electrochemical Reduction of Carbon Dioxide by Iron(0) Porphyrins. Synergistic Effect of Lewis Acid Cations. *J. Phys. Chem.* **1996**, *100*, 19981–19985. [[CrossRef](#)]
- Lei, K.; Xia, B.Y. Electrocatalytic CO₂ Reduction: From Discrete Molecular Catalysts to Their Integrated Catalytic Materials. *Chem. Eur. J.* **2022**, *28*, e202200141.
- Amanullah, S.; Saha, P.; Nayek, A.; Ahmed, M.E.; Dey, A. Biochemical and Artificial Pathways for the Reduction of Carbon Dioxide, Nitrite and the Competing Proton Reduction: Effect of 2nd Sphere Interactions in Catalysis. *Chem. Soc. Rev.* **2021**, *50*, 3755–3823. [[CrossRef](#)]
- Gotico, P.; Leibl, W.; Halime, Z.; Aukauloo, A. Shaping the Electrocatalytic Performance of Metal Complexes for CO₂ Reduction. *ChemElectroChem* **2021**, *8*, 3472–3481. [[CrossRef](#)]
- Nichols, A.W.; Machan, C.W. Secondary-Sphere Effects in Molecular Electrocatalytic CO₂ Reduction. *Front. Chem.* **2019**, *7*, 397. [[CrossRef](#)] [[PubMed](#)]
- Costentin, C.; Drouet, S.; Robert, M.; Savéant, J.-M. A Local Proton Source Enhances CO₂ Electroreduction to CO by a Molecular Fe Catalyst. *Science* **2012**, *338*, 90–94. [[CrossRef](#)]
- Azcarate, I.; Costentin, C.; Robert, M.; Savéant, J.-M. Dissection of Electronic Substituent Effects in Multielectron–Multistep Molecular Catalysis. Electrochemical CO₂-to-CO Conversion Catalyzed by Iron Porphyrins. *J. Phys. Chem. C* **2016**, *120*, 28951–28960. [[CrossRef](#)]
- Azcarate, I.; Costentin, C.; Robert, M.; Savéant, J.-M. Through-Space Charge Interaction Substituent Effects in Molecular Catalysis Leading to the Design of the Most Efficient Catalyst of CO₂-to-CO Electrochemical Conversion. *J. Am. Chem. Soc.* **2016**, *138*, 16639–16644. [[CrossRef](#)]
- Hammouche, M.; Lexa, D.; Savéant, J.M. Catalysis of the Electrochemical Reduction of Carbon Dioxide by Iron("0") Porphyrins. *J. Electroanal. Chem.* **1988**, *249*, 347–351. [[CrossRef](#)]
- Mondal, B.; Rana, A.; Sen, P.; Dey, A. Intermediates Involved in the 2e[−]/2H⁺ Reduction of CO₂ to CO by Iron(0) Porphyrin. *J. Am. Chem. Soc.* **2015**, *137*, 11214–11217. [[CrossRef](#)]
- Nichols, E.M.; Derrick, J.S.; Nistanaki, S.K.; Smith, P.T.; Chang, C.J. Positional Effects of Second-Sphere Amide Pendants on Electrochemical CO₂ Reduction Catalyzed by Iron Porphyrins. *Chem. Sci.* **2018**, *9*, 2952–2960. [[CrossRef](#)]
- Margarit, C.G.; Schnedermann, C.; Asimow, N.G.; Nocera, D.G. Carbon Dioxide Reduction by Iron Hangman Porphyrins. *Organometallics* **2019**, *38*, 1219–1223. [[CrossRef](#)]
- Guo, K.; Li, X.; Lei, H.; Zhang, W.; Cao, R. Unexpected Effect of Intramolecular Phenolic Group on Electrocatalytic CO₂ Reduction. *ChemCatChem* **2020**, *12*, 1591–1595. [[CrossRef](#)]
- Guo, H.; Liang, Z.; Guo, K.; Lei, H.; Wang, Y.; Zhang, W.; Cao, R. Iron Porphyrin with Appended Guanidyl Group for Significantly Improved Electrocatalytic Carbon Dioxide Reduction Activity and Selectivity in Aqueous Solutions. *Chin. J. Catal.* **2022**, *43*, 3089–3094. [[CrossRef](#)]
- Sen, P.; Mondal, B.; Saha, D.; Rana, A.; Dey, A. Role of 2nd Sphere H-bonding Residues in Tuning the Kinetics of CO₂ Reduction to CO by Iron Porphyrin Complexes. *Dalton Trans.* **2019**, *48*, 5965–5977. [[CrossRef](#)] [[PubMed](#)]
- Gotico, P.; Boitrel, B.; Guillot, R.; Sircoglou, M.; Quaranta, A.; Halime, Z.; Leibl, W.; Aukauloo, A. Second-Sphere Biomimetic Multipoint Hydrogen-Bonding Patterns to Boost CO₂ Reduction of Iron Porphyrins. *Angew. Chem. Int. Ed.* **2019**, *58*, 4504–4509. [[CrossRef](#)]

25. Gotico, P.; Roupnel, L.; Guillot, R.; Sircoglou, M.; Leibl, W.; Halime, Z.; Aukauloo, A. Atropisomeric Hydrogen Bonding Control for CO₂ Binding and Enhancement of Electrocatalytic Reduction at Iron Porphyrins. *Angew. Chem. Int. Ed.* **2020**, *59*, 22451–22455. [[CrossRef](#)] [[PubMed](#)]
26. Derrick, J.S.; Loipersberger, M.; Nistanaki, S.K.; Rothweiler, A.V.; Head-Gordon, M.; Nichols, E.M.; Chang, C.J. Templating Bicarbonate in the Second Coordination Sphere Enhances Electrochemical CO₂ Reduction Catalyzed by Iron Porphyrins. *J. Am. Chem. Soc.* **2022**, *144*, 11656–11663. [[CrossRef](#)] [[PubMed](#)]
27. Liu, G.; Fan, Y.-J.; Zhang, J.-L. Construction of Secondary Coordination Sphere Boosts Electrochemical CO₂ Reduction of Iron Porphyrins. *J. Porphyr. Phthaloc.* **2020**, *24*, 465–472. [[CrossRef](#)]
28. Amanullah, S.; Saha, P.; Dey, A. Activating the Fe(I) State of Iron Porphyrinoid with Second-Sphere Proton Transfer Residues for Selective Reduction of CO₂ to HCOOH via Fe(III/II)–COOH Intermediate(s). *J. Am. Chem. Soc.* **2021**, *143*, 13579–13592. [[CrossRef](#)]
29. Guo, K.; Li, X.; Lei, H.; Guo, H.; Jin, X.; Zhang, X.-P.; Zhang, W.; Apfel, U.-P.; Cao, R. Role-Specialized Division of Labor in CO₂ Reduction with Doubly-Functionalized Iron Porphyrin Atropisomers. *Angew. Chem. Int. Ed.* **2022**, *61*, e202209602. [[CrossRef](#)]
30. Ramuglia, A.R.; Budhija, V.; Ly, K.H.; Marquardt, M.; Schwalbe, M.; Weidinger, I.M. An Iron Porphyrin Complex with Pendant Pyridine Substituents Facilitates Electrocatalytic CO₂ Reduction via Second Coordination Sphere Effects. *ChemCatChem* **2021**, *13*, 3934–3944. [[CrossRef](#)]
31. Narouz, M.R.; De La Torre, P.; An, L.; Chang, C.J. Multifunctional Charge and Hydrogen-Bond Effects of Second- Sphere Imidazolium Pendants Promote Capture and Electrochemical Reduction of CO₂ in Water Catalyzed by Iron Porphyrins. *Angew. Chem. Int. Ed.* **2022**, *61*, e202207666. [[CrossRef](#)]
32. Costentin, C.; Robert, M.; Savéant, J.-M. Catalysis of the Electrochemical Reduction of Carbon Dioxide. *Chem. Soc. Rev.* **2013**, *42*, 2423–2436. [[CrossRef](#)] [[PubMed](#)]
33. Gotico, P.; Halime, Z.; Aukauloo, A. Recent Advances in Metalloporphyrin-Based Catalyst Design Towards Carbon Dioxide Reduction: From Bio-Inspired Second Coordination Sphere Modifications to Hierarchical Architectures. *Dalton Trans.* **2020**, *49*, 2381–2396. [[CrossRef](#)] [[PubMed](#)]

Disclaimer/Publisher’s Note: The statements, opinions and data contained in all publications are solely those of the individual author(s) and contributor(s) and not of MDPI and/or the editor(s). MDPI and/or the editor(s) disclaim responsibility for any injury to people or property resulting from any ideas, methods, instructions or products referred to in the content.